Journal of Geophysical Research: Atmospheres

Supporting Information for

Stratocumulus Precipitation Properties over the Southern Ocean Observed from Aircraft during the SOCRATES campaign

L. Kang[1], R. T. Marchand [1], and R. Wood[1]

1 Department of Atmospheric Sciences, University of Washington, Seattle, Washington, USA

Contents of this file

Figures S1 to S11

Introduction

Figure S1 is a schematic showing the typical flight module during the SOCRATES campaign. Figure S2 shows an example of the zenith pointing Doppler velocity fields from RF13 before and after the correction of the zenith pointing data. Figure S3 shows the comparison between mean velocity profiles for nadir pointing and zenith pointing data from RF13 before and after the correcting the zenith pointing data. Figure S4 shows the Mie-to-Rayleigh backscatter ratio. Figure S5 shows probability and cumulative density functions of below-cloud lidar particle linear depolarization ratio (PLDR) for all warm-topped clouds. Figure S6 shows an example case from research flight 10 (RF10) on 2018 Feb. 8th during 02:42-02:52 UTC. Figure S7 shows Z-R relationships derived rain rate. Figure S8-10 shows ZV retrieved the median equivolumetric diameter D_0, precipitation number N_{precip}, and rain rate, respectively, assuming different shape factor μ. Figure S11 shows an example case with radar-lidar retrieved rain rate and rain rate derived from the exponential fitting the retrieved rain rates and extrapolate to the aircraft level.

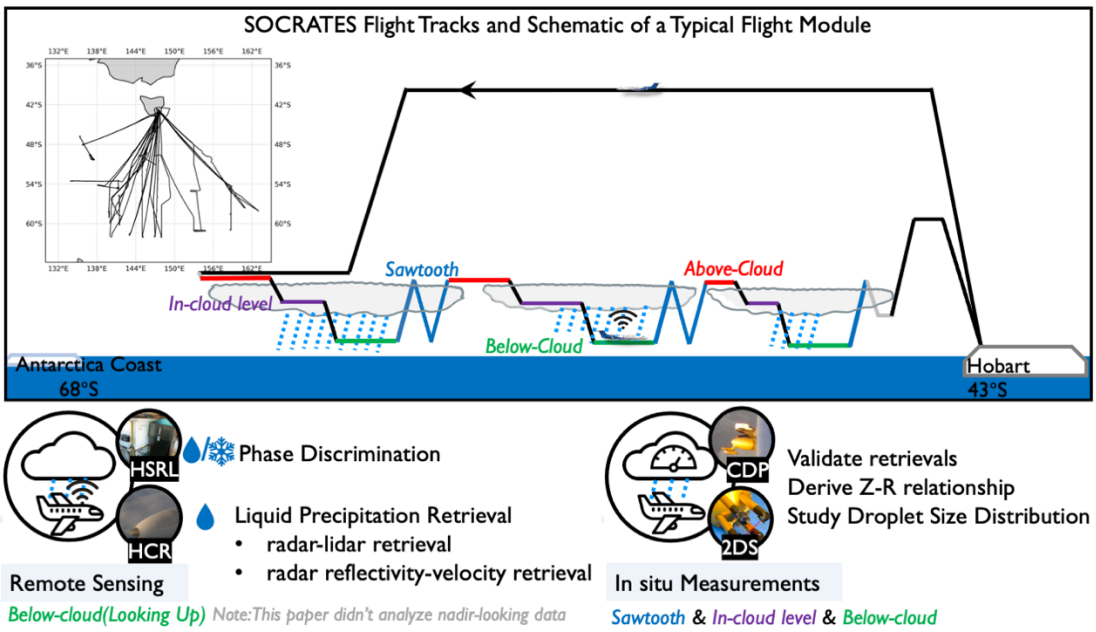

Figure S1. A schematic showing the typical flight module during the SOCRATES campaign (with flight tracks map embedded). The black lines show the flight tracks, with different segments highlighted: below-cloud level legs in green; above-cloud level legs in red; sawtooth legs in blue; in-cloud level legs in purple. The graphics below the schematic summarize the main instruments and how the remote sensing and in situ data from different segments were used in this study.

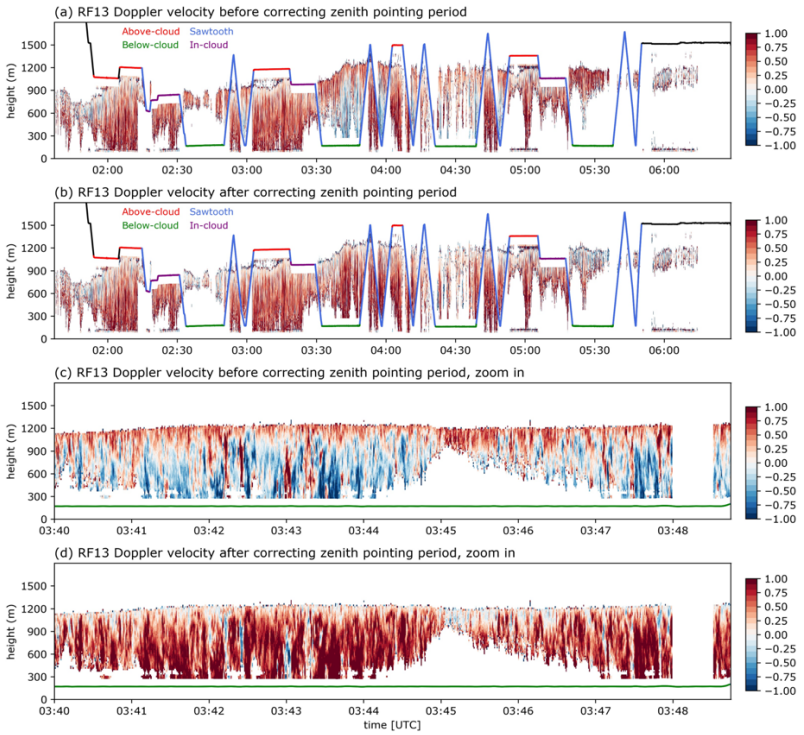

Figure S2. An example of the zenith pointing Doppler velocity fields from RF13 (a) before and (b) after the correction of the zenith pointing data, as well as the zoom in view for zenith-pointing period starting from 03:40 UTC time (c) before and (d) after the correction.

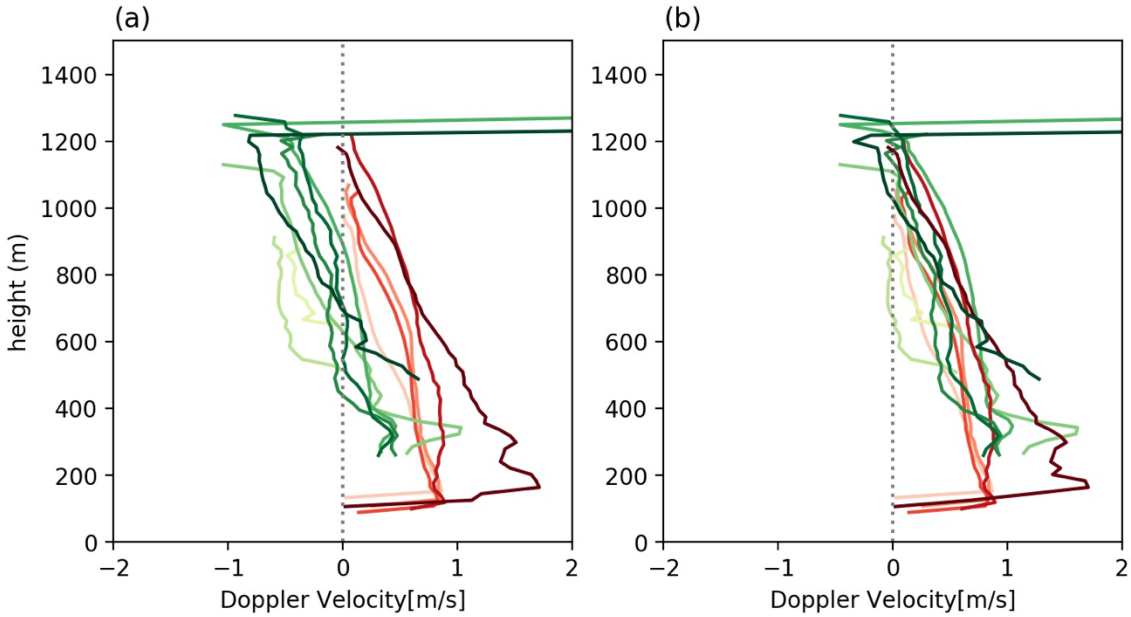

Figure S3. Mean velocity profiles for nadir pointing and zenith pointing data from RF13

(a) before the correcting and (b) after the correcting the zenith pointing data. Here each profile represents the average mean velocity profile averaged over either nadir pointing times (denoted as red) or zenith pointing times (denoted as green). The vertical dashed line represents the 0 m s^{-1} for reference.

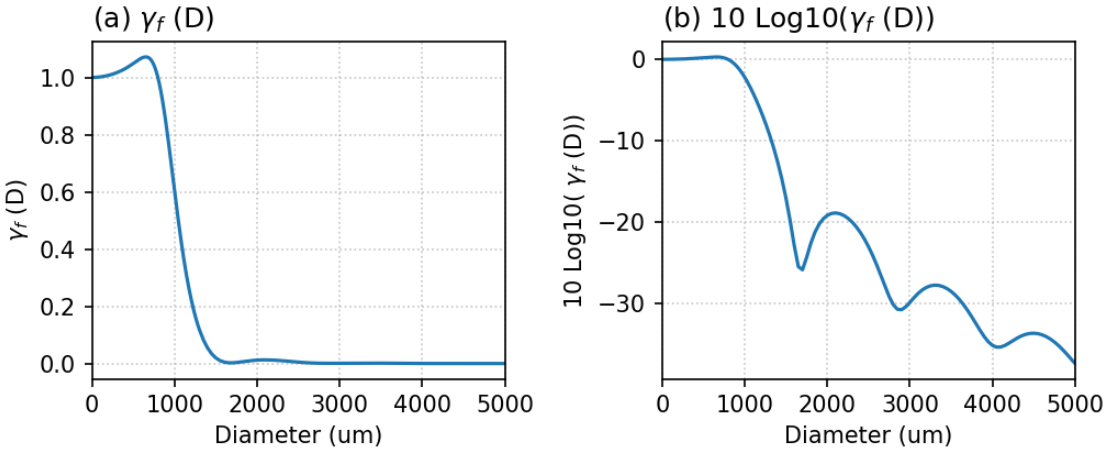

Figure S4. The Mie-to-Rayleigh backscatter ratio (a) $\boldsymbol{\gamma_f(D)}$, and (b) 10 $\boldsymbol{log_{10}(\gamma_f(D))}$. $\boldsymbol{\gamma_f(D)}$ is the ratio of the backscatter efficiency of Mie scattering for W-band (94-GHz), calculated using miepython package that based on Wiscombe(1979), and backscatter efficiency of Rayleigh scattering (Bohren & Huffman, 1983).

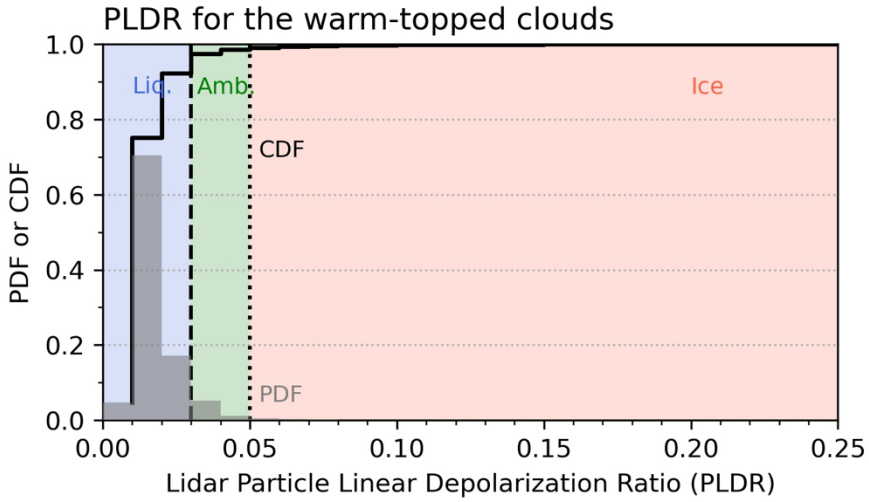

Figure S5. Probability and cumulative density functions of below-cloud lidar particle linear depolarization ratio (PLDR) for all warm-topped clouds (when cloud top temperature >

0°C). To distinguish different precipitation type, liquid precipitation is marked as blue, ice precipitation is marked as red, and ambiguous precipitation is marked as green.

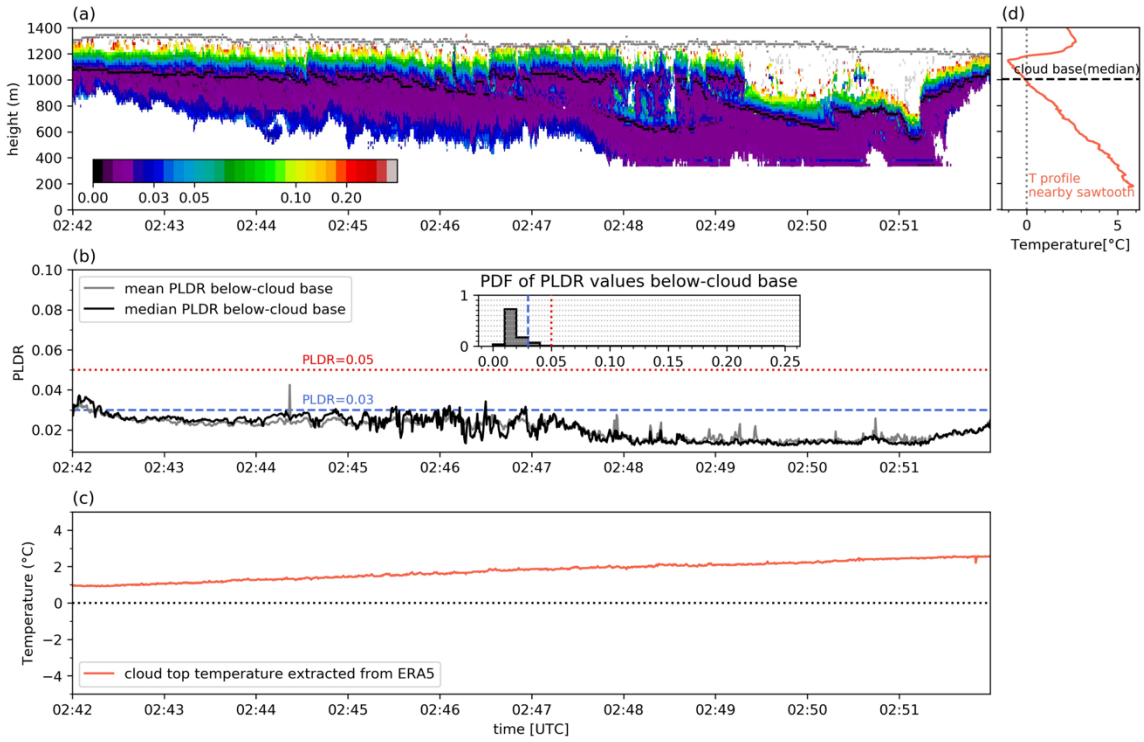

Figure S6. An example case from research flight 10 (RF10) on 2018 Feb. 8th during 02:42-02:52 UTC with (a) lidar particle linear depolarization ratio (PLDR), (b) time series of median PLDR (black) or mean PLDR (grey) values below-cloud base, and the probability density function (PDF) of PLDR values below-cloud base, (c) the cloud top temperature extracted from ERA5 reanalysis data, and (d) temperature profile measured by aircraft from a adjacent sawtooth leg (2018 Feb. 8th during 02:52-02:58 UTC). The grey dotted line in panel

c and d represents 0°C for reference. Blue and red line on panel b shows the threshold or PLDR equals 0.03 or 0.05.

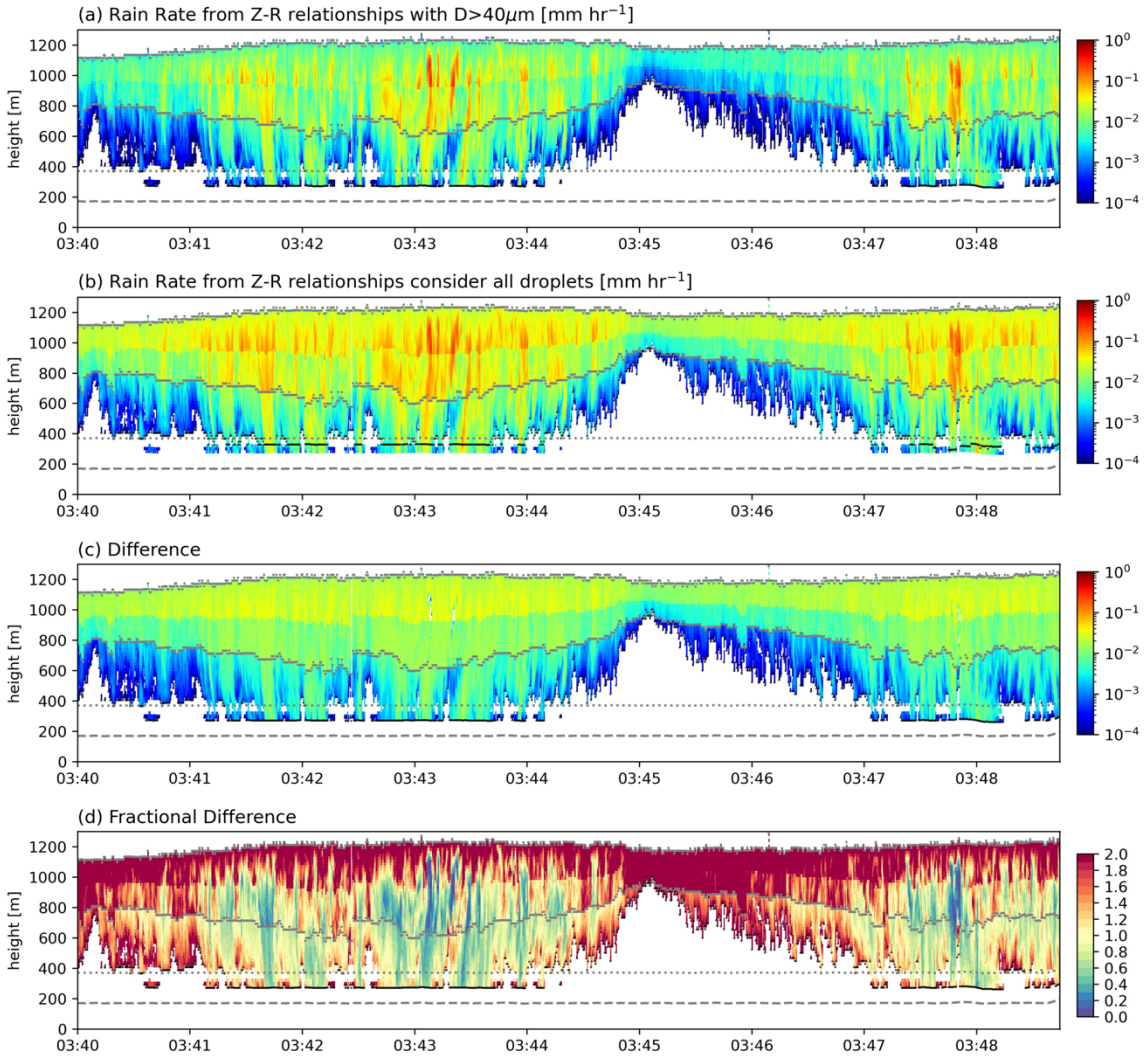

Figure S7. Z-R relationships derived rain rate. Panel a use the Z-R relationships that has D >40 μm cutoff, while Z-R relationships used in panel b does not apply any cutoff, and

considers all droplet sizes. Panel c shows difference calculated as $RR_{panel\ b}$ - $RR_{panel\ a}$. Panel d shows the fractional difference calculated as ($RR_{panel\ b}$ - $RR_{panel\ a}$) / $RR_{panel\ a}$

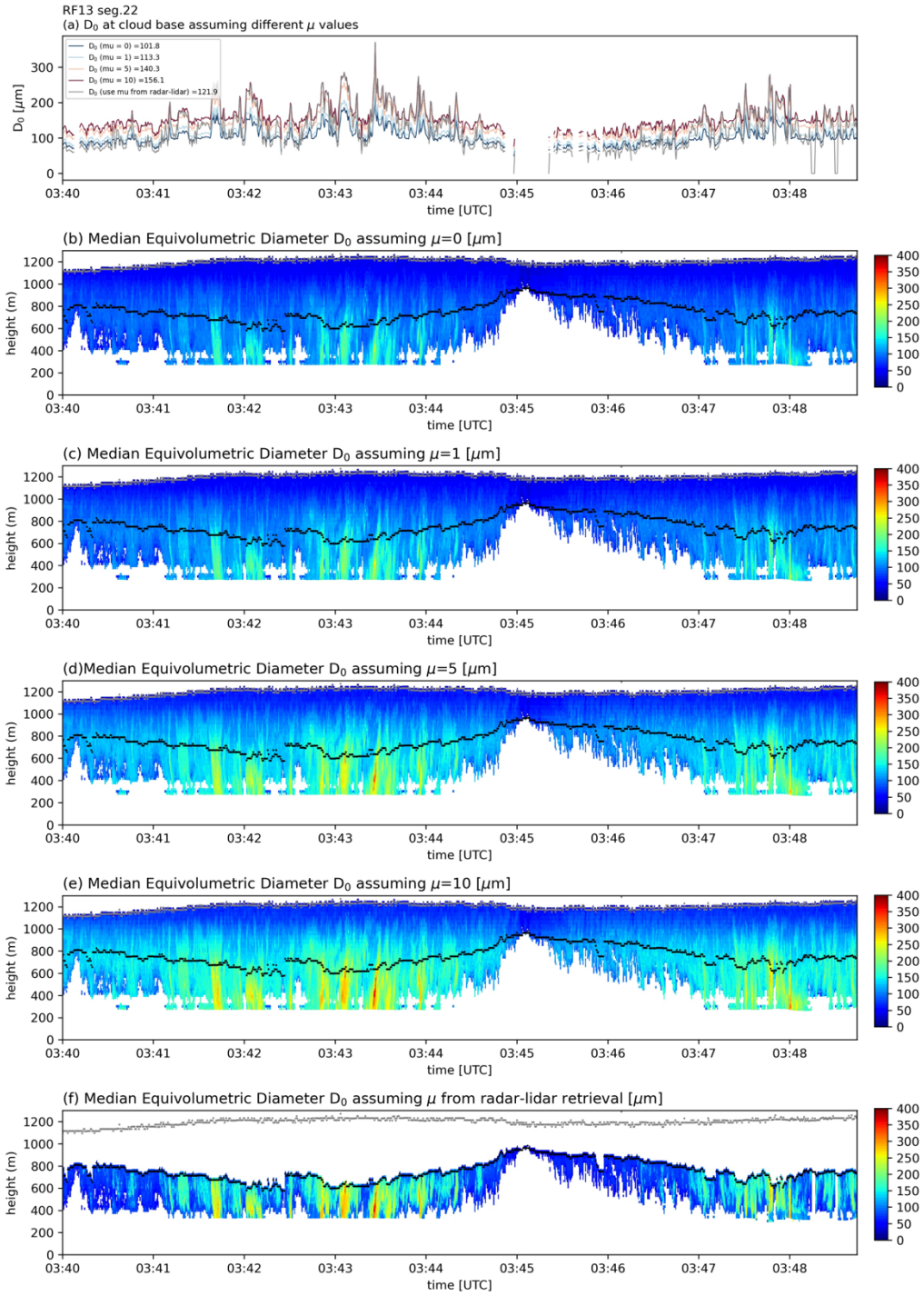

Figure S8. ZV retrieved median equivolumetric diameter D_0 assuming different shape factor $\boldsymbol{\mu}$

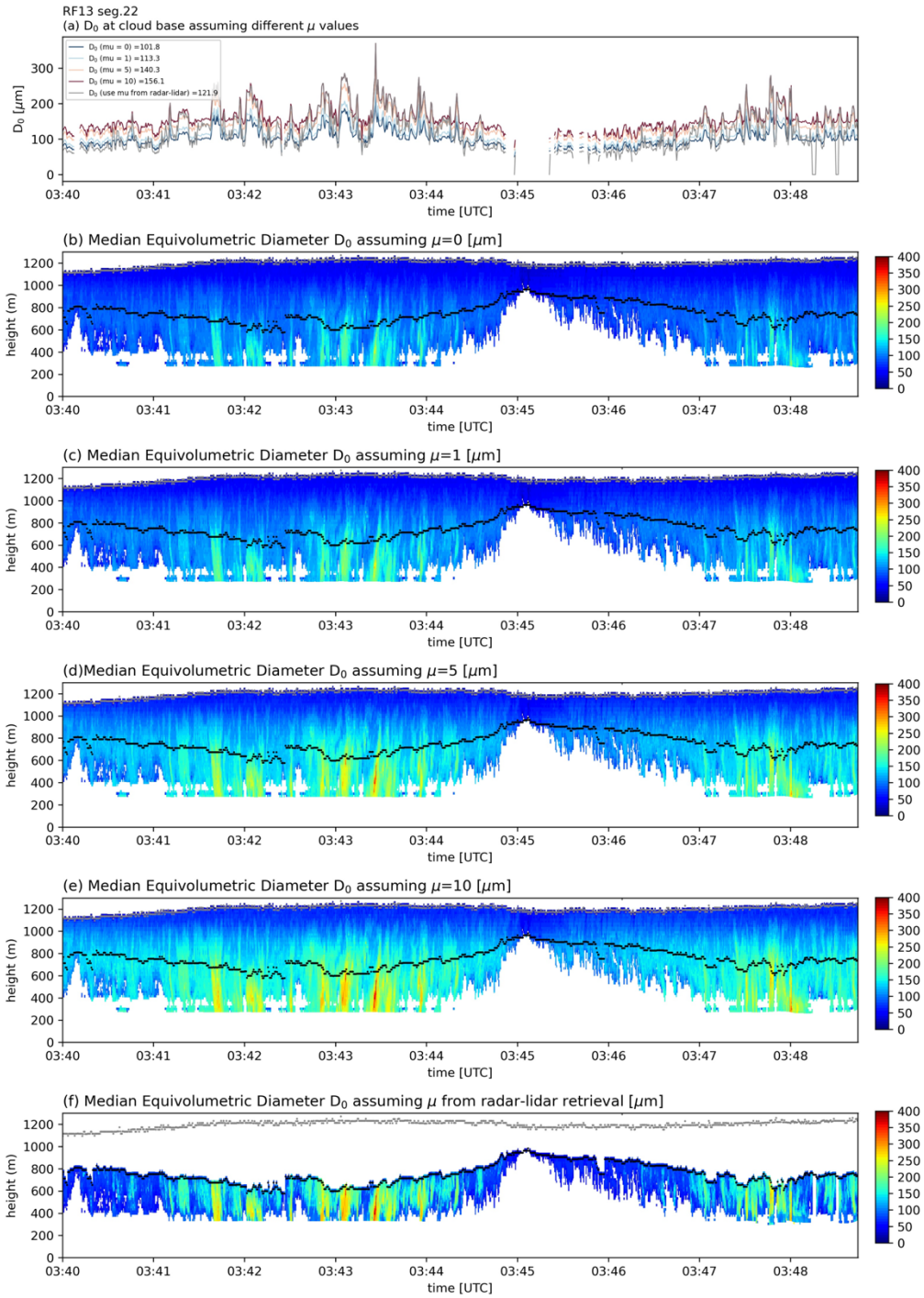

Figure S9. ZV retrieved precipitation number concentration N_{precip} assuming different shape factor $\boldsymbol{\mu}$

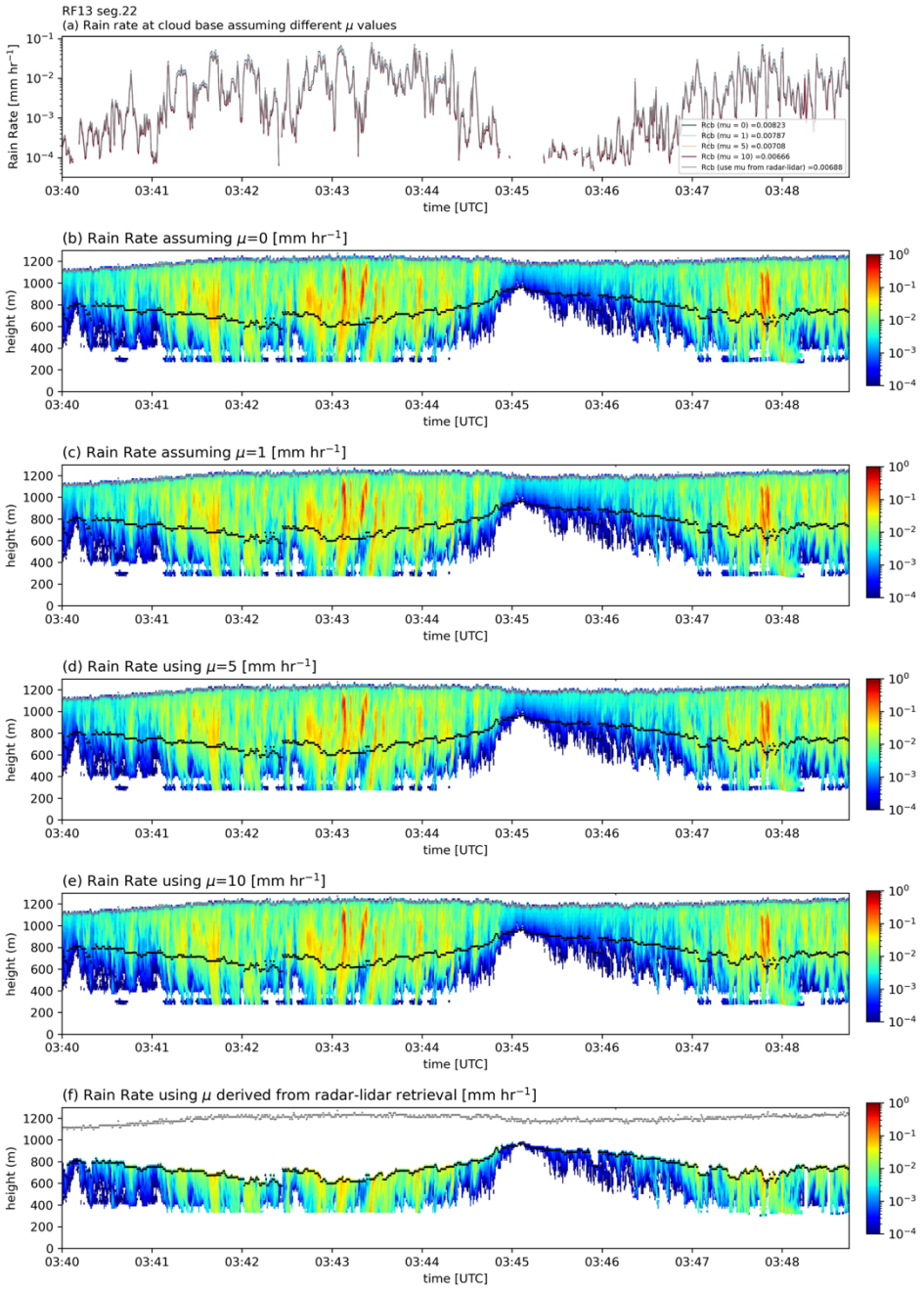

Figure S10. ZV retrieved rain rate assuming different shape factor $\boldsymbol{\mu}$

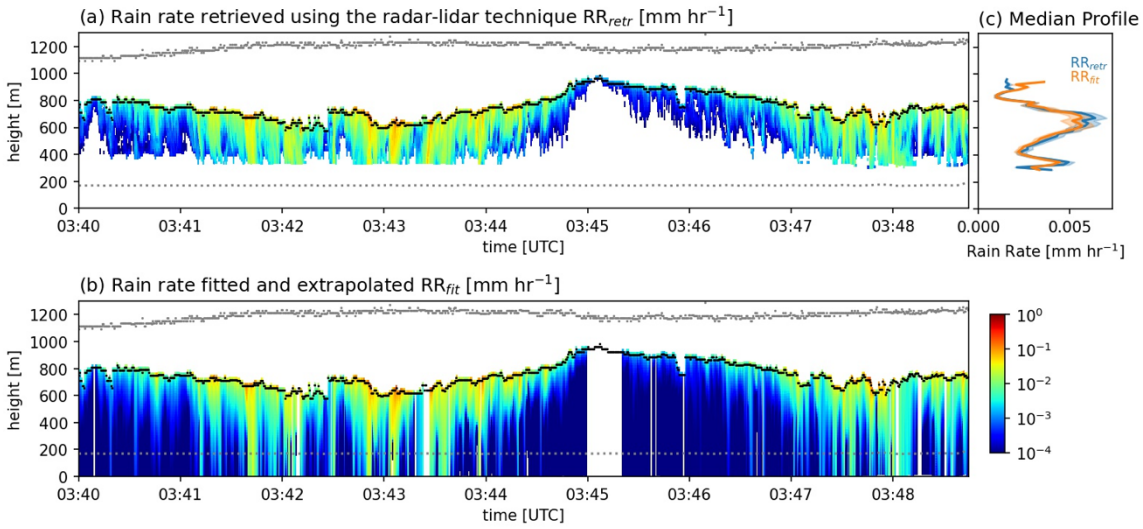

Figure S11. An example case with (a) radar-lidar retrieved rain rate, (b) rain rate derived from the exponential fitting the retrieved rain rates and extrapolate to the aircraft level (marked as the dashed line), and (c) median rain rate profiles of from radar-lidar retrieval (blue) or exponentially fit (orange). In the panel c, the median profiles are calculated over the area where radar-lidar retrieved rain rate are available.